

Effect of Spin-Texture Dynamics on Three-Dimensional Orbital Dirac Semimetals

Pritam Chatterjee¹ and Anirudha Menon^{2,*}

¹*Department of Physics, The University of Tokyo,
7-3-1 Hongo, Bunkyo-ku, Tokyo 113-0033, Japan*

²*Centre for Theoretical and Computational Physics,
National Yang Ming Chiao Tung University, Hsinchu City, Taiwan*

(Dated: January 27, 2026)

We consider the minimal coupling of a Dirac semimetal Hamiltonian to a generic spin-texture in this work. A simple unitary transformation gauges away the spatial dependence in the exchange term, leading to the generation of effective corrections to the Dirac dispersion. A full function's worth of freedom is obtained as a result. Choosing different pitch vectors, we show that many forms of novel phenomena arise in such systems. For example, a linear pitch vector leads to the generation of type-I Weyl semimetal — we observe the anomalous Hall effect and the chiral magnetic effect. The anomalous Hall coefficient requires a non-zero pitch vector whereas the CME is proportional to the exchange coupling. The band structure of the model in the presence of a magnetic field shows a Lifshitz transition. The introduction of a suitable time dependent pitch vector leads to the formation of nodal spheres in the Sambe space of effective Hamiltonians. This nodal sphere is robust to all orders in van-Vleck perturbation theory as proven explicitly.

Introduction. Topological semimetals [1–13] have been studied extensively by the condensed matter community since their first predictions over a decade ago. This class of materials exhibits point- or line-like degeneracies arising from band touchings between the conduction and valence bands near the Fermi energy. Prominent examples include Dirac semimetals [6–9], Weyl semimetals [2–5], and nodal-line semimetals [10–13], realized in both spinless and spinful systems. Here, “spinless” refers to electronic systems in which spin-orbit coupling (SOC) can be effectively neglected [14], rendering spin a passive degeneracy. While these phases have been widely explored using theoretical and computational approaches, not all of them have been connected to experimentally viable material platforms.

Dirac semimetals (DSMs) are characterized by four linearly dispersing bands meeting at a point-like degeneracy known as the Dirac point. Although the total Chern number associated with a Dirac point vanishes identically, the Berry phase accumulated along symmetry-allowed loops encircling the node is quantized to π . Dirac points are generally unstable against perturbations and may gap out or split into pairs of Weyl points unless protected by crystalline symmetries [14]. Spinful DSMs, in which SOC plays a central role, have been studied extensively, with experimental realizations reported in Cd_3As_2 and Na_3Bi . In contrast, spinless DSMs preserve full $\text{SU}(2)$ spin-rotation symmetry and have been discussed primarily from the perspective of representation theory [6, 15]. One reason this class has received comparatively less attention is the absence of a general microscopic guiding principle for realizing band inversion—an essential ingredient for topological semimetals—in the absence of SOC. Moreover, until recently, few material candidates had been proposed for spinless DSMs. Despite these challenges, spinless DSMs are promising plat-

forms for hosting a range of exotic physical phenomena, as we demonstrate in this work.

Recently, non-collinear magnetic textures and other unconventional magnetic orders have emerged as versatile platforms for engineering fundamental physical phenomena in condensed matter systems and for advancing spintronics applications. Electrons coupled to non-collinear magnetic textures experience emergent (fictitious) gauge fields, including axial electromagnetic fields [16–22]. Spatial or temporal variations in (anti)ferromagnetic order lead to a broad range of electronic responses beyond those found in systems with uniform and static magnetism. Such non-collinear spin configurations can give rise to phenomena including the anomalous Hall effect (AHE) and the chiral magnetic effect (CME) [16, 22–28]. Furthermore, the coupling between emergent gauge fields from magnetic textures and superconducting order parameters has been shown to generate rich physics, including topological superconductivity hosting Majorana end, edge, and corner modes [29–35]. Non-collinear magnetism thus provides an alternative route for engineering chirality and topology in solids without the need for external gauge fields or laser drives.

There has been some work on the interaction of topological semimetals with spin-textures [36, 37] but there are many gaps in the literature. In this work, we consider the effect of spin-textures on orbital DSMs leading to host of novel phenomena including the appearance of Weyl points and nodal spheres. We explore the emergent anomalous Hall effect, the chiral magnetic effect, and the induced Lifshitz transition in the magnetic band structure.

Model and Unitary Rotation. We begin with a spinless Dirac semimetal minimal model Hamiltonian coupled to a spin-texture exchange term of the form

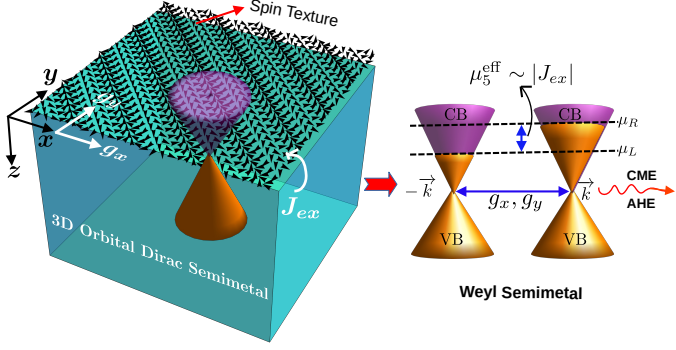


FIG. 1. Schematic illustrating the signatures of the CME and AHE in an effective Weyl spectrum originating from a 3D orbital Dirac semimetal under spin-texture dynamics.

$$H(\vec{k}, \vec{r}) = v_F \sigma_0 (\vec{\tau} \cdot \vec{k}) + J_{ex} \vec{S}(\vec{r}) \cdot \vec{\sigma}, \quad (1)$$

where $\vec{\tau}$ is a valley degree of freedom, $\vec{\sigma}$ is real spin, and \vec{S} represents a classical spin. v_F represents the so called Fermi velocity of the DSM and J_{ex} represents the strength of the spin-texture coupling. Such a model may be derived from microscopic theories of interfaces using the Schreiffer-Wolf class of transformations. We assume the following form for \vec{S} :

$$\vec{S}(\vec{r}) = |\vec{S}| [\sin \theta \cos \phi, \sin \theta \sin \phi, \cos \theta]. \quad (2)$$

in spherical coordinates and set $\theta(r) = \pi/2$ without loss of generality. This leads to a dependence of the \vec{S} vector purely on $\phi(r)$. We choose a form for ϕ as $\phi(r) \equiv \phi(x, y)$, such that $\partial_z \phi = 0$.

A natural unitary transformation presents itself as $U(r) = \exp \left[-i \frac{\phi(r)}{2} \sigma_z \otimes \tau_0 \right]$ to re-express the Hamiltonian in a convenient form with the exchange term being simplified to a position independent term. Under this transformation, the Dirac piece transforms as

$$\begin{aligned} U^\dagger(r) v_F \tau_i k_i U(r) &= v_F \tau_i U^\dagger(r) k_i U(r) \\ &= -i v_F \tau_i U^\dagger(r) \partial_i U(r) \\ &= -i v_F \tau_i [U^\dagger(r) U(r) \partial_i \\ &\quad + U^\dagger(r) \{\partial_i U(r)\}] \\ &= -i v_F \tau_i [U^\dagger(r) U(r) \partial_i \\ &\quad - i \frac{1}{2} U^\dagger(r) U(r) \partial_i \phi(r) \sigma_z] \\ &= v_F \tau_i [k_i - \frac{1}{2} \partial_i \phi \sigma_z], \end{aligned} \quad (3)$$

where $U^\dagger U = 1$ and we've dropped the dependence of ϕ on r . Naturally, the Dirac term then looks like

$$\begin{aligned} U^\dagger H_{DSM} U &= v_F \sigma_0 (\vec{\tau} \cdot \vec{k}) \\ &\quad - \frac{1}{2} \sigma_z [\tau_x \partial_x \phi + \tau_y \partial_y \phi]. \end{aligned} \quad (4)$$

Next, we look at the effect of the unitary rotation on the exchange spin-texture piece, which is well known, and it turns out that

$$U^\dagger J_{ex} \vec{\sigma} \cdot \vec{S} U = J_{ex} |\vec{S}| \sigma_x. \quad (5)$$

With this, the full transformed Hamiltonian $H_t \equiv U^\dagger H U$ takes the form

$$\begin{aligned} H_t &= v_F \sigma_0 (\vec{\tau} \cdot \vec{k}) - \frac{1}{2} \sigma_z [\tau_x \partial_x \phi + \tau_y \partial_y \phi] \\ &\quad + J_{ex} |\vec{S}| \sigma_x. \end{aligned} \quad (6)$$

The transformation is remarkable — we now have a DSM Hamiltonian with some extra terms which may induce novel physics into the system. We are free to choose the form of the pitch vector ϕ , and indeed different cases have been explored for such vectors in the literature.

Linear Pitch vector Induced WSM. We may now choose a simple form for the pitch vector as a warm up. We find such a simple choice to be $\phi(r) = g_x x + g_y y$. In this case the derivatives work out trivially and we see that we get a Hamiltonian of the form

$$\begin{aligned} H_t &= v_F \sigma_0 (\vec{\tau} \cdot \vec{k}) - \frac{1}{2} \sigma_z [g_x \tau_x + g_y \tau_y] \\ &\quad + J_{ex} |\vec{S}| \sigma_x. \end{aligned} \quad (7)$$

We set $|\vec{S}| = 1$ for convenience. This Hamiltonian may be diagonalized by the *squaring trick* as is well known in the literature. The details can be found in the supplementary material. We find that the eigenvalues take the form

$$\epsilon_{\pm, \rho}(\mathbf{k}) = \rho \sqrt{v_F^2 k^2 + J^2 + \frac{g^2}{4}} \pm v_F \sqrt{\mathcal{A}(k)}, \quad (8)$$

where, $\mathcal{A}(k) = 4J^2 k^2 + (\mathbf{k} \cdot \mathbf{g})^2$ with $\mathbf{g} = (g_x, g_y, 0)$ and $\rho = \pm 1$, is an index obtained by the diagonalization of the $\vec{\tau}$ subspace obtained after squaring. While it is not apparent, one can show that this dispersion corresponds to the existence of two pairs of Weyl points, a pair at $\vec{k} = (\frac{g_x}{g v_F} \sqrt{J^2 + (g/2)^2}, \frac{g_y}{g v_F} \sqrt{J^2 + (g/2)^2}, 0)$ and a pair at $\vec{k} = 0$ but separated in energy.

We show the spectrum in Fig. 2 where we can see that the four-band system remains untilted. We have

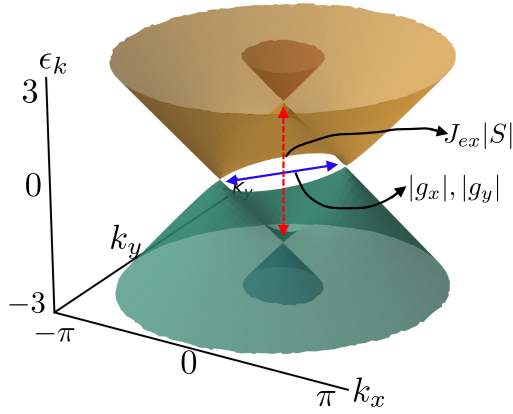


FIG. 2. Full energy spectrum from Eq. (8) for an inversion-asymmetric Weyl spectrum in the k_x - k_y plane with $J_{ex} = 1$, $g_x = g_y = \pi/2$, $k_z = 0$, and $v_F = 1$.

verified that the monopole charges of the Weyl nodes in each case numerically, and they work out to be ± 1 (see supplementary file).

The existence of the two Weyl points separated in momentum space signals the existence of an anomalous Hall current. The Hall conductivity is determined by the integral of the Berry curvature Ω_{ij} as

$$\sigma_{ij} = -\frac{e^2}{\hbar} \sum_n \int \frac{d^d k}{(2\pi)^d} f_n(\mathbf{k}) \Omega_{ij}^{(n)}(\mathbf{k}), \quad (9)$$

where n is a sum over bands, d is the spacetime dimension, and $f(\vec{k})$ is the Fermi-Dirac distribution. It then follows that the Hall conductivity at $T = 0$ is given purely by the topological term since there is no tilt to be coupled to the chemical potential. The final expression for the conductivity tensor follows trivially from previous works [1, 38, 39] as

$$\begin{aligned} \sigma_{yz} &= \frac{e^2}{2\pi^2 \hbar g v_F} \sqrt{J^2 + (g/2)^2} \\ \sigma_{xz} &= \frac{e^2}{2\pi^2 \hbar g v_F} \sqrt{J^2 + (g/2)^2}, \\ \sigma_{xy} &= 0, \end{aligned} \quad (10)$$

where $g = |\vec{g}| = \sqrt{g_x^2 + g_y^2}$. Noticeably, the results depend on both the pitch vector and the strength of the exchange coupling J , suggesting that the origin of this effect is the breaking of *time reversal symmetry* by the spin

texture. One can see that if either g_x or g_y is zero, the respective Hall conductivity component vanishes, showing that the pitch vector is the driving element in the occurrence of this phenomenon, whereas J adds to the strength of the effect but cannot generate it on its own. Further, if we assume $g_x = g \cos \eta$ and $g_y = g \sin \eta$, then

$$\begin{aligned} \sigma_{yz} &= \frac{e^2}{2\pi^2 \hbar v_F} \frac{1}{\sqrt{J^2 + (g/2)^2}} \cos \eta \\ \sigma_{xz} &= \frac{e^2}{2\pi^2 \hbar v_F} \frac{1}{\sqrt{J^2 + (g/2)^2}} \sin \eta. \end{aligned} \quad (11)$$

We see that there is in a sense a rotational invariance as we change the angle η and hence the components of g - the sum in quadrature of the non-zero Hall conductivities is unchanged as $\sqrt{\sigma_{xz}^2 + \sigma_{yz}^2} = \frac{e^2}{2\pi^2 \hbar v_F} \frac{1}{\sqrt{J^2 + (g/2)^2}}$. There are then circles of constant Hall conductivity in the (g_x, g_y) plane.

We introduce now a magnetic field in the z -direction to study the possibility of the chiral magnetic effect [39–44] in this model. Using the symmetric gauge $\mathbf{A} = (-By/2, Bx/2, 0)$ and defining $\pi_x = -i\hbar\partial_x + eA_x$, $\pi_y = -i\hbar\partial_y + eA_y$, we construct the ladder operators

$$a = \frac{\ell_B}{\sqrt{2\hbar}} (\pi_x - i\pi_y), \quad a^\dagger = \frac{\ell_B}{\sqrt{2\hbar}} (\pi_x + i\pi_y), \quad (12)$$

where $\ell_B = \sqrt{\frac{\hbar}{eB}}$ is the magnetic length. The Landau-level spinor ansatz is chosen as

$$\Psi_n = \begin{pmatrix} u_\uparrow |n-1\rangle \\ v_\uparrow |n\rangle \\ u_\downarrow |n-1\rangle \\ v_\downarrow |n\rangle \end{pmatrix}, \quad (13)$$

ensuring that all appearances of a and a^\dagger reduce to \sqrt{n} . Projecting to the Landau level basis with $\Omega_n = v_F \sqrt{2n\hbar/\ell_B}$, the Hamiltonian becomes

$$H_n = \begin{pmatrix} v k_z & \Omega_n - \frac{g}{2} & J_{ex} & 0 \\ \Omega_n - \frac{g}{2} & -v k_z & 0 & J_{ex} \\ J_{ex} & 0 & v k_z & \Omega_n + \frac{g}{2} \\ 0 & J_{ex} & \Omega_n + \frac{g}{2} & -v k_z \end{pmatrix}, \quad (14)$$

with $v \equiv v_F \hbar$. The Hamiltonian may be diagonalized by the squaring trick to yield the eigenvalues. Thus, the energy spectrum for $n \geq 1$ is

$$\epsilon_n^{(s,\delta)}(k_z) = s \sqrt{v_F^2 k_z^2 + \Omega_n^2 + \frac{g^2}{4} + J_{ex}^2 + \delta \sqrt{4v_F^2 k_z^2 J_{ex}^2 + 4\Omega_n^2 J_{ex}^2 + g^2 \Omega_n^2}}, \quad (15)$$

with $s = \pm$ and $\lambda = \pm$. For $n = 0$,

$$\epsilon_0^s(k_z) = s |v_F k_z - J_{ex}|. \quad (16)$$

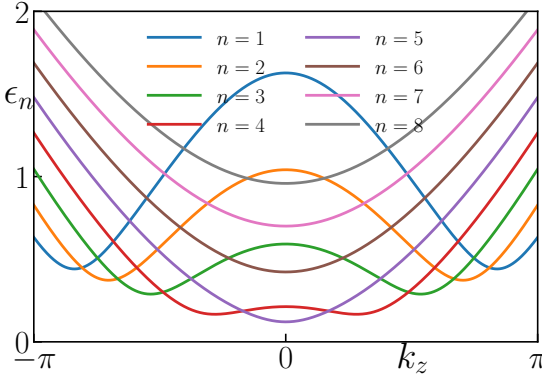


FIG. 3. Landau-quantized band structure as a function of the longitudinal momentum k_z for several Landau indices n . Each Landau level splits into four branches due to exchange hybridization, labeled by (s, δ) . While higher-index subbands exhibit a conventional single-minimum dispersion with a band edge at $k_z = 0$, the lower hybridized branch develops a double-minimum structure with degenerate band minima at finite $\pm k_z^*$. Parameters used are $J_{ex} = 3$, $g = 1$, $s = +1$, $\delta = -1$, $l_B = 1$ and $\hbar = v_F = 1$.

One cannot obtain this result by simply substituting $n = 0$ in Eqn.(15) - care needs to be taken to project onto the ground state manifold.

In a magnetic field, the spectrum (as shown in Fig.3) reorganizes into Landau sub-bands that disperse along the field direction k_z . Exchange coupling hybridizes the two spin sectors of each Landau level, yielding four branches per index n with energies $\epsilon_n^{(s,\delta)}(k_z)$. While high-index sub-bands exhibit the conventional single-minimum Dirac-like dispersion with a band edge at $k_z = 0$, the lower hybridized branch undergoes a qualitative reconstruction at small n . Specifically, the competition between the Landau quantization scale Ω_n and the exchange energy J_{ex} drives a transition from a single minimum at $k_z = 0$ to a double-minimum structure with degenerate band minima at finite $\pm k_z^*$. This exchange-driven reconstruction constitutes a Lifshitz transition within an individual Landau sub-band, changing the number of Fermi points at fixed chemical potential without breaking any symmetry. As a consequence, additional one-dimensional van Hove singularities appear in the density of states, and new extremal orbits emerge, leading to field-tunable anomalies in quantum oscillations and thermodynamic response.

We had introduced the magnetic field in the hope of detecting the CME and to this end, the current response

to the applied magnetic field can be calculated via [39] as

$$j_z = -\frac{e}{2\pi l_B^2} \lim_{\Lambda \rightarrow \infty} \int_{-\Lambda}^{\Lambda} \frac{dk_z}{2\pi} \frac{\partial}{\partial z} \left[\epsilon_0^- + \sum_{n=1}^{\infty} \sum_{s=\pm} \epsilon_n^{s,-} \right]. \quad (17)$$

The contribution from the higher Landau levels vanish by symmetry and we are simply left with the contribution of the lowest LL. The derivative and the integral annihilate leaving us to evaluate the limit appropriately.

$$j_z = -\frac{e^2 B}{4\pi^2} [\epsilon_0^-(\Lambda) - \epsilon_0^-(-\Lambda)] \quad (18)$$

Inserting the appropriate energy terms into the expression above, we find that $\epsilon_0^-(\Lambda) - \epsilon_0^-(-\Lambda) = -|v_F \Lambda - J| + | -v_F \Lambda - J| = -v_F \Lambda + J + v_F \Lambda + J = 2J$. Thus, the chiral magnetic parameter μ_5^{eff} is given by

$$\mu_5^{\text{eff}} = \frac{j_z}{B} = -\frac{e^2}{2\pi^2} J_{ex}. \quad (19)$$

Time Dependent Pitch Vector. We now consider the case where the pitch vector has time-dependence, and it takes the form $\phi(r, t) = g[x \cos \omega t + \lambda y \sin \omega t]$. The algebra for the unitary transformation changes accordingly and is $H \rightarrow H' = U^\dagger H U - i U^\dagger \partial_t U = U^\dagger H U - \frac{1}{2} (\partial_t \phi) \sigma_z$. Thus, the transformed Hamiltonian takes the form

$$\begin{aligned} H'(r, t) = v_F & \left[\tau_x \left(k_x - \frac{1}{2} g \cos \omega t \sigma_z \right) \right. \\ & + \tau_y \left(k_y - \frac{\lambda}{2} g \sin \omega t \sigma_z \right) + \tau_z k_z \left. \right] \\ & + J_{ex} |\vec{S}| \sigma_x + \frac{\omega g}{2} [x \sin \omega t - \lambda y \cos \omega t] \sigma_z. \end{aligned} \quad (20)$$

While it may look like this Hamiltonian is equivalent to a DSM under the influence of circularly polarized light and a Zeeman field, we remind the reader that $\vec{\nabla} \phi$ is curl-less. Floquet systems have been studied previously in the context of topological semimetals [45–47], although the results we present here are novel. We may now choose a regime where $\omega \gg \Delta E$, where ΔE is the bandwidth of the system and then invoke the van-Vleck expansion given by

$$H_{\text{eff}} = H_0^F + \frac{[H_{-1}^F, H_{+1}^F]}{\omega} + \mathcal{O}(\frac{1}{\omega^2}), \quad (21)$$

to leading order in perturbation theory, where $H_n^F = \frac{1}{T} \int_0^T H(t) e^{in\omega t} dt$. It may appear that the $U\partial_t U$ term may lead to position dependencies in the effective Hamiltonian, but a simple calculation shows that this dependence is removed. The effective Floquet Hamiltonian in this setup is then given by

$$H_{\text{eff}} = v_F \left[\tau_x k_x + \tau_y k_y + \tau_z (k_z - \lambda \frac{v_F^2 g^2}{4\omega}) \right] + J_{ex} |\vec{S}| \sigma_z. \quad (22)$$

The Hamiltonian may be trivially diagonalized to get that the energies are given by

$$\epsilon_{s,t}(k) = s J_{ex} |\vec{S}| + t v_F \sqrt{k_x^2 + k_y^2 + (k_z - \lambda \frac{v_F^2 g^2}{4\omega})^2}, \quad (23)$$

where $s, t = \pm$ gives the four distinct bands. Then we can see that when $s \cdot t < 0$, there is the existence of a nodal sphere at $E = 0$ specified by the equation $k_x^2 + k_y^2 + (k_z - \lambda \frac{v_F^2 g^2}{4\omega})^2 = J_{ex}^2 \vec{S}^2$. This nodal sphere is a rare and unique topological phenomenon and we will now demonstrate that it appears at all orders in van-Vleck perturbation theory - there is no operator which gaps it out.

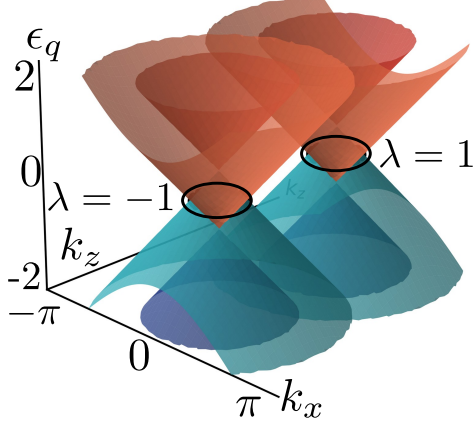


FIG. 4. The Floquet bulk spectrum of a nodal-ring semimetal for $\lambda = \pm 1$ in the k_x - k_z plane is shown, resulting from coupled temporal and spatial spin-texture dynamics in a three-dimensional orbital Dirac semimetal. Parameters used are $J_{ex} = 0.5$, $g_x = g_y = 2.5$, $k_y = 0$, $\omega = 1$, and $v_F = 1$.

A crucial structural property of the unitarily transformed Hamiltonian is that

$$[H'(t), \sigma_z] = 0 \quad \forall t. \quad (24)$$

That is, the driven Hamiltonian possesses an exact $U(1)$ spin-rotation symmetry about the z -axis, and the operator σ_z is conserved at all times.

The van Vleck effective Hamiltonian is constructed entirely from time averages and nested commutators of $H'(t)$:

$$H_{\text{eff}} = H^{(0)} + H^{(1)} + H^{(2)} + \dots, \\ H^{(n)} \sim \sum [\![H'(t_1), H'(t_2)], \dots, H'(t_{n+1})]\!], \quad (25)$$

where $[\![\cdot]\!]$ denotes an n -fold nested commutator. Using Eq. (24), every commutator appearing in $H^{(n)}$ also commutes with σ_z . Therefore,

$$[H_{\text{eff}}, \sigma_z] = 0 \quad \text{to all orders in } 1/\omega. \quad (26)$$

Equation (26) implies that H_{eff} is exactly block diagonal in the eigenbasis of σ_z . Each block describes an independent Weyl Hamiltonian,

$$H_{\pm}(\mathbf{k}) = \mathbf{v} \cdot (\mathbf{k} - \mathbf{k}_0) \cdot \boldsymbol{\tau} \pm \Delta, \quad (27)$$

where the velocities \mathbf{v} , the Weyl-node shift \mathbf{k}_0 , and the energy offset Δ are renormalized by higher-order terms in the van-Vleck expansion. The quasienergy bands in the two blocks satisfy

$$\epsilon_{\pm, \pm}(\mathbf{k}) = \pm \Delta \pm |\mathbf{v} \cdot (\mathbf{k} - \mathbf{k}_0)|. \quad (28)$$

The condition $E_{\pm, \mp}(\mathbf{k}) = 0$ therefore defines a closed two-dimensional surface in momentum space,

$$|\mathbf{v} \cdot (\mathbf{k} - \mathbf{k}_0)| = \Delta, \quad (29)$$

which reduces to a perfect sphere at leading order and becomes a deformed ellipsoid upon including higher-order corrections. Because the two σ_z sectors remain strictly decoupled at all orders, no term capable of hybridizing the bands on this surface is ever generated. As a result, the nodal surface (Eqn. 29) is an exact feature of the full van-Vleck effective Hamiltonian to all orders in $1/\omega$, although its shape is renormalized by sub-leading corrections.

In the absence of spin-mixing terms, the Floquet-engineered Hamiltonian enjoys an exact $U(1)$ symmetry generated by σ_z , which persists to all orders in the van-Vleck expansion. This symmetry enforces a block-diagonal structure with two energy-shifted Weyl cones and guarantees a stable nodal surface (sphere/ellipsoid) in the quasi-energy spectrum. Generic perturbations that break this $U(1)$ symmetry hybridize the two sectors and reduce the nodal surface to isolated Weyl points or fully gap it.

Conclusions. In this work, we examined the effects of coupling a spin-texture to a spinless Dirac semimetal. We employed a unitary transformation to find a Hamiltonian whose spectrum and eigenstates were controlled by the pitch vector and exchange coupling. Using a linear pitch vector led to the formation of four Weyl nodes,

two at distinct momenta space and the other two split in energy. This novel system exhibited the classic anomalous Hall and chiral magnetic effects characteristic of Weyl systems. The topological Hall response exhibited a circle of invariance in the (g_x, g_y) plane, whereas the CME remained proportional to the exchange coupling J_{ex} . Along the way, we found the magnetic-field-induced Landau level structure exhibited a Lifshitz transition as we increased the Landau index n . We then chose a time-dependent pitch vector and analyzed the resulting system using van-Vleck perturbation theory. We found that the system hosted emergent nodal spheres in the Sambe space of effective Hamiltonians — these spheres were protected by a $U(1)$ symmetry and would remain closed surfaces to all orders in perturbation theory. This last result was explicitly proven. The novel results of this work invites experimental exploration further supported by the recent discovery of the material family Pr_8CoGa_3 which hosts spinless Dirac fermions.

AM and PC contribute equally to this project. Pritam Chatterjee acknowledges Prof. Arijit Saha, Prof. Kenji Fukushima, and Prof. Takashi Oka for useful discussions. AM would like to thank NCTS Taiwan for their continuing support of his postdoctoral work.

343, 864 (2014).

- [8] Z. Wang, Y. Sun, X.-Q. Chen, C. Franchini, G. Xu, H. Weng, X. Dai, and Z. Fang, Dirac semimetal and topological phase transitions in A_3Bi ($\text{A} = \text{Na}, \text{K}, \text{Rb}$), *Phys. Rev. B* **85**, 195320 (2012).
- [9] M. Neupane, S.-Y. Xu, R. Sankar, N. Alidoust, G. Bian, C. Liu, I. Belopolski, T.-R. Chang, H.-T. Jeng, H. Lin, A. Bansil, F. Chou, and M. Z. Hasan, Observation of a three-dimensional topological dirac semimetal phase in high-mobility Cd_3As_2 , *Nature Communications* **5**, 3786 (2014).
- [10] Y. Kim, B. J. Wieder, C. L. Kane, and A. M. Rappe, Dirac line nodes in inversion-symmetric crystals, *Phys. Rev. Lett* **115**, 036806 (2015).
- [11] R. Yu, H. Weng, Z. Fang, X. Dai, and X. Hu, Topological node-line semimetal and dirac semimetal state in antiperovskite Cu_3PdN , *Phys. Rev. Lett* **115**, 036807 (2015).
- [12] M. Hirayama, R. Okugawa, T. Miyake, and S. Murakami, Topological dirac nodal lines and surface charges in fcc alkaline earth metals, *Nature Communications* **8**, 14022 (2017).
- [13] R. Takahashi, M. Hirayama, and S. Murakami, Spinless hourglass nodal-line semimetals, *Phys. Rev. B* **96**, 155206 (2017).
- [14] M. Sato, J. Bouaziz, S. Sumita, S. Kobayashi, I. Tateishi, S. Blügel, A. Furusaki, and M. Hirayama, Ideal spin-orbit-free dirac semimetal and diverse topological transitions in Pr_8CoGa_3 family, *Communications Materials* **5**, 253 (2024).
- [15] B.-J. Yang and N. Nagaosa, Classification of stable three-dimensional dirac semimetals with nontrivial topology, *Nature Communications* **5**, 4898 (2014).
- [16] Y. Araki, Magnetic textures and dynamics in magnetic weyl semimetals, *Annalen der Physik* **532**, 1900287 (2020).
- [17] P. Bruno, V. K. Dugaev, and M. Taillefumier, Topological hall effect and berry phase in magnetic nanostructures, *Phys. Rev. Lett.* **93**, 096806 (2004).
- [18] T. Schulz, R. Ritz, A. Bauer, M. Halder, M. Wagner, C. Franz, C. Pfleiderer, K. Everschor, M. Garst, and A. Rosch, Emergent electrodynamics of skyrmions in a chiral magnet, *Nature Physics* **8**, 301 (2012).
- [19] N. Nagaosa and Y. Tokura, Emergent electromagnetism in solids, *Physica Scripta* **2012**, 014020 (2012).
- [20] C.-X. Liu, P. Ye, and X.-L. Qi, Chiral gauge field and axial anomaly in a weyl semimetal, *Phys. Rev. B* **87**, 235306 (2013).
- [21] A. Ozawa, Y. Araki, and K. Nomura, Chiral gauge field in fully spin-polarized magnetic weyl semimetal with magnetic domain walls, *Journal of the Physical Society of Japan* **93**, 094704 (2024).
- [22] R. Ilan, A. G. Grushin, and D. I. Pikulin, Pseudo-electromagnetic fields in 3d topological semimetals, *Nature Reviews Physics* **2**, 29 (2020).
- [23] R. Terasawa and H. Ishizuka, Anomalous hall effect by chiral spin textures in the two-dimensional luttinger model, *Phys. Rev. B* **109**, L060407 (2024).
- [24] Y. Ishihara, T. Mizushima, A. Tsuruta, and S. Fujimoto, Torsional chiral magnetic effect due to skyrmion textures in a weyl superfluid ${}^3\text{He}-\text{A}$, *Phys. Rev. B* **99**, 024513 (2019).
- [25] L. An, X. Zhu, W. Gao, M. Wu, W. Ning, and M. Tian, Chiral anomaly and nontrivial berry phase in the topo-

* menon.cond.mat@gmail.com

- [1] N. P. Armitage, E. J. Mele, and A. Vishwanath, Weyl and dirac semimetals in three-dimensional solids, *Rev. Mod. Phys.* **90**, 015001 (2018).
- [2] S.-Y. Xu, N. Alidoust, I. Belopolski, Z. Yuan, G. Bian, T.-R. Chang, H. Zheng, V. N. Strocov, D. S. Sanchez, G. Chang, C. Zhang, D. Mou, Y. Wu, L. Huang, C.-C. Lee, S.-M. Huang, B. Wang, A. Bansil, H.-T. Jeng, T. Neupert, A. Kaminski, H. Lin, S. Jia, and M. Z. Hasan, Discovery of a weyl fermion state with fermi arcs in niobium arsenide, *Nature Physics* **11**, 748 (2015).
- [3] L. X. Yang, Z. K. Liu, Y. Sun, H. Peng, H. F. Yang, T. Zhang, B. Zhou, Y. Zhang, Y. F. Guo, M. Rahn, D. Prabhakaran, Z. Hussain, S.-K. Mo, C. Felser, B. Yan, and Y. L. Chen, Weyl semimetal phase in the non-centrosymmetric compound taas, *Nature Physics* **11**, 728 (2015).
- [4] B. Q. Lv, H. M. Weng, B. B. Fu, X. P. Wang, H. Miao, J. Ma, P. Richard, X. C. Huang, L. X. Zhao, G. F. Chen, Z. Fang, X. Dai, T. Qian, and H. Ding, Experimental discovery of weyl semimetal taas, *Phys. Rev. X* **5**, 031013 (2015).
- [5] H. Weng, C. Fang, Z. Fang, B. A. Bernevig, and X. Dai, Weyl semimetal phase in noncentrosymmetric transition-metal monophosphides, *Phys. Rev. X* **5**, 011029 (2015).
- [6] S. M. Young, S. Zaheer, J. C. Y. Teo, C. L. Kane, E. J. Mele, and A. M. Rappe, Dirac semimetal in three dimensions, *Phys. Rev. Lett.* **108**, 145405 (2012).
- [7] Z. K. Liu, B. Zhou, Y. Zhang, Z. J. Wang, H. M. Weng, D. Prabhakaran, S.-K. Mo, Z. X. Shen, Z. Fang, X. Dai, Z. Hussain, and Y. L. Chen, Discovery of a three-dimensional topological dirac semimetal Na_3Bi , *Science*

- logical nodal-line semimetal SrAs_3 , *Phys. Rev. B* **99**, 045143 (2019).
- [26] M. Redies, F. R. Lux, J.-P. Hanke, P. M. Buhl, S. Blügel, and Y. Mokrousov, Mixed topology ring states for hall effect and orbital magnetism in skyrmions of weyl semimetals, *Phys. Rev. B* **102**, 184407 (2020).
- [27] S. Heidari, R. Asgari, and D. Culcer, Probing domain wall dynamics in magnetic weyl semimetals via the non-linear anomalous hall effect, *Phys. Rev. B* **107**, 214450 (2023).
- [28] A. Harada and H. Ishizuka, Spin motive force by the momentum-space berry phase in magnetic weyl semimetals, *Phys. Rev. B* **107**, 195202 (2023).
- [29] R. Hess, H. F. Legg, D. Loss, and J. Klinovaja, Prevalence of trivial zero-energy subgap states in nonuniform helical spin chains on the surface of superconductors, *Phys. Rev. B* **106**, 104503 (2022).
- [30] P. Chatterjee, S. Banik, S. Bera, A. K. Ghosh, S. Pradhan, A. Saha, and A. K. Nandy, Topological superconductivity by engineering noncollinear magnetism in magnet/superconductor heterostructures: A realistic prescription for the two-dimensional kitaev model, *Phys. Rev. B* **109**, L121301 (2024).
- [31] P. Chatterjee, A. K. Ghosh, A. K. Nandy, and A. Saha, Second-order topological superconductor via noncollinear magnetic texture, *Phys. Rev. B* **109**, L041409 (2024).
- [32] M. Subhadarshini, A. Pal, P. Chatterjee, and A. Saha, Multiple topological phase transitions unveiling gapless topological superconductivity in magnet/unconventional superconductor hybrid platform, *Applied Physics Letters* **124**, 183102 (2024).
- [33] P. Chatterjee, S. Pradhan, A. K. Nandy, and A. Saha, Tailoring the phase transition from topological superconductor to trivial superconductor induced by magnetic textures of a spin chain on a *p*-wave superconductor, *Phys. Rev. B* **107**, 085423 (2023).
- [34] R. Brüning, J. Bedow, R. Lo Conte, K. von Bergmann, D. K. Morr, and R. Wiesendanger, The noncollinear path to two-dimensional topological superconductivity, *ACS Nano* **19**, 36215 (2025).
- [35] M. Subhadarshini, A. Pal, P. Chatterjee, and A. Saha, Identifying majorana edge and end modes in a josephson junction of a *p*-wave superconductor with a magnetic barrier, *Phys. Rev. B* **112**, 115439 (2025).
- [36] Y. Araki and K. Nomura, Charge pumping induced by magnetic texture dynamics in weyl semimetals, *Phys. Rev. Appl.* **10**, 014007 (2018).
- [37] S. Bera and S. John, Spin-flux skyrmions: Anomalous electron dynamics and spin-hall currents (2025), arXiv:2511.19239 [cond-mat.mes-hall].
- [38] A. Menon and B. Basu, Anomalous hall transport in tilted multi-weyl semimetals, *Journal of Physics: Condensed Matter* **33**, 045602 (2020).
- [39] A. Menon, S. Chatopadhyay, and B. Basu, Chiral magnetic effect in lattice models of tilted multi-weyl semimetals, *Phys. Rev. B* **104**, 075129 (2021).
- [40] A. A. Zyuzin and A. A. Burkov, Topological response in weyl semimetals and the chiral anomaly, *Phys. Rev. B* **86**, 115133 (2012).
- [41] M.-C. Chang and M.-F. Yang, Chiral magnetic effect in the absence of weyl node, *Phys. Rev. B* **92**, 205201 (2015).
- [42] M.-C. Chang and M.-F. Yang, Chiral magnetic effect in a two-band lattice model of weyl semimetal, *Phys. Rev. B* **91**, 115203 (2015).
- [43] K. Fukushima, D. E. Kharzeev, and H. J. Warringa, Chiral magnetic effect, *Phys. Rev. D* **78**, 074033 (2008).
- [44] S. Ebihara, K. Fukushima, and T. Oka, Chiral pumping effect induced by rotating electric fields, *Phys. Rev. B* **93**, 155107 (2016).
- [45] H. Hübener, M. Sentef, and U. De Giovannini, Creating stable floquet–weyl semimetals by laser-driving of 3d dirac materials, *Nature Communications* **8**, 13940 (2017).
- [46] A. Menon, D. Chowdhury, and B. Basu, Photoinduced tunable anomalous hall and nernst effects in tilted weyl semimetals using floquet theory, *Phys. Rev. B* **98**, 205109 (2018).
- [47] T. Nag, A. Menon, and B. Basu, Thermoelectric transport properties of floquet multi-weyl semimetals, *Phys. Rev. B* **102**, 014307 (2020).